International Journal of Heat and Technology
Vol. 44, No. 2, April, 2026, pp. 491-503
Journal homepage: http://iieta.org/journals/ijht

Thermo-Mechanical Performance of a Rib-Reinforced Polymer Oil Pan for Diesel Engine Applications

Tomas Condori, John Huacasi, Pascual Adriazola, Waygand Beltran, Christofer Diaz*

Universidad Nacional de San Agustín de Arequipa, Arequipa 04000, Peru

Corresponding Author Email: cdiazar@unsa.edu.pe

https://doi.org/10.18280/ijht.440205

Received: 28 January 2026
Revised: 26 March 2026
Accepted: 8 April 2026
Available online: 30 April 2026

Keywords:
deformation, oil pan, polymer material, reinforcement ribs, sealing performance, stress analysis, structural stiffness, thermal effects

ABSTRACT

This study investigates the thermo-mechanical performance of an engine oil pan manufactured from recycled polyamide 66 reinforced with 35% glass fiber (rPA66-GF35). The transition from metallic to polymer-based components is often hindered by the reduction in elastic modulus at high operating temperatures. Using coupled thermo-mechanical finite element analysis (FEA), the baseline polymer geometry was evaluated at 140 °C, revealing a critical factor of safety (FoS) of 0.47 due to bending-dominated deformation. A geometry-driven stiffness recovery strategy was implemented by integrating an external rib network designed to act as primary load paths. Results demonstrate that the reinforced configuration successfully redistributes von Mises stresses, reducing typical shell stresses from 86 MPa to 29.6 MPa. This optimization achieved a FoS of 1.35 and an 11.5% reduction in critical deformations with a marginal mass increase of only 4.12%. It is concluded that topology-based reinforcement effectively compensates for thermal softening, restoring structural integrity. Furthermore, comparative benchmarking against a reference cast aluminum design demonstrates that the optimized polymer configuration achieves a 40% mass reduction while maintaining acceptable sealing-line deformation, validating its mass-normalized stiffness. The optimized polymer design demonstrates structural viability, making it a viable alternative to conventional metal casings in lightweight engines.

1. INTRODUCTION

The automotive industry is undergoing a progressive transition toward lightweight and sustainable vehicle architectures, driving the replacement of conventional metallic components with polymer-based solutions [1]. In recent years, major manufacturers such as Mercedes-Benz, BMW, Peugeot, and Citroën have introduced plastic oil pans in selected vehicle platforms, replacing traditional cast aluminum designs. This shift is primarily motivated by the significant weight reduction potential of polymers, their improved noise, vibration, and harshness (NVH) behavior [2, 3], and the lower carbon footprint associated with polymer processing when compared to aluminum casting routes [4, 5].

Despite their increasing industrial adoption, the scientific and technical information regarding polymer oil pans remains remarkably limited. In most cases, manufacturers do not disclose the specific polymer grades, fiber reinforcement levels, or thermal–mechanical limits of the materials employed. As a result, critical parameters such as maximum operating temperature, stiffness degradation under thermal exposure, long-term sealing performance, and impact resistance are poorly documented in the open literature. This lack of transparency creates a substantial knowledge gap between industrial practice and academic understanding, hindering independent validation and broader adoption of polymer oil pan technologies [6, 7].

From an engineering standpoint, the oil pan is a safety-critical component exposed to a combination of demanding operating conditions. It must maintain hermetic sealing to prevent oil leakage, withstand sustained exposure to elevated oil temperatures, resist mechanical loads induced by engine vibrations, and tolerate accidental impacts from road debris or uneven terrain [8, 9]. Additionally, internal structural features such as baffles must simultaneously contribute to oil flow control and structural stiffness, further complicating the design requirements. However, comprehensive studies addressing the coupled thermal, structural, and dynamic behavior of polymer oil pans across these diverse loading environments remain scarce [8, 10].

In this context, the present study aims to contribute to the limited body of knowledge by evaluating a recycled glass-fiber-reinforced polyamide (rPA66-GF35) as a candidate material for oil pan applications under critical thermal and mechanical conditions [11, 12]. Rather than relying on empirical assumptions, the work focuses on quantifying the thermo-structural response, sealing performance, and impact resistance of the polymer design, providing insight into the feasibility and limitations of polymer oil pans as sustainable alternatives to conventional aluminum components.

To clearly define the scope of the present study and establish a realistic engineering context, the oil pan analyzed corresponds to a Cummins 4BT 3.9 diesel engine, a four-cylinder inline power unit widely used in light commercial

vehicles, industrial equipment, and urban-duty applications. The engine delivers a nominal power output of 75 kW (105 hp) at 2400 rpm, with a total displacement of 3.9 liters, making it a representative platform for evaluating oil pan performance under demanding thermal and mechanical conditions [13].

Figure 1 illustrates the reference engine considered in this investigation. Figure 1(a) shows the real Cummins 4BT 3.9 engine assembly, while Figure 1(b) presents an isometric Computer-Aided Design (CAD) view of the same engine, where the oil pan under investigation is highlighted in yellow. These visual representations are intended to provide the reader with a clear understanding of the oil pan location, orientation, and geometric relevance within the overall powertrain architecture, without introducing modeling or manufacturing assumptions at this stage.

(a) Real Cummins 4BT 3.9 diesel engine assembly

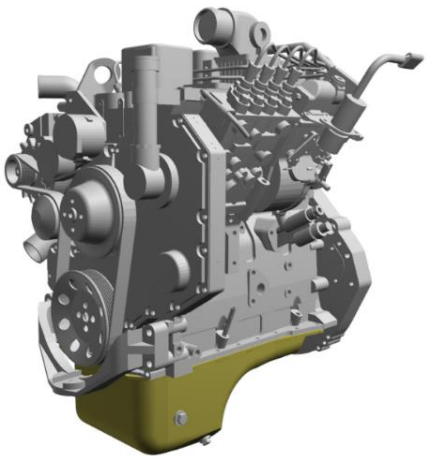

(b) Isometric Computer-Aided Design (CAD) view of the Cummins 4BT 3.9 engine with the oil pan highlighted

Figure 1. Reference Cummins 4BT 3.9 engine configuration

The Cummins B-Series engines are characterized by a compact and robust design philosophy, enabling compliance with current emission standards while maintaining mechanical simplicity. In addition, these engines are specifically engineered for low noise emission, allowing operation in high-density urban environments such as commercial and residential districts. This characteristic makes the oil pan not only a structural and thermal component, but also a contributor to the overall NVH behavior of the powertrain [14].

The oil pan is mounted at the lowest region of the engine assembly, where it is continuously exposed to elevated lubricant temperatures, mechanical constraints imposed by the engine block, and external environmental hazards such as road debris and uneven terrain. These combined conditions impose stringent requirements on stiffness retention, sealing integrity, and impact resistance, particularly when considering the substitution of cast aluminum with polymer-based materials.

Key technical specifications of the Cummins 4BT 3.9 engine are summarized in Table 1. These parameters provide the necessary background for defining the thermal boundary conditions, oil volume, and mechanical loading scenarios applied in the thermo-structural and optimization analyses presented in the following sections.

Table 1. Technical specifications of the Cummins 4BT 3.9 engine [13]

Parameter	Specification
Engine model	Cummins 4BT 3.9
Number of cylinders	4 cylinders (inline)
Displacement	3.9 L
Bore	102 mm
Stroke	120 mm
Rated power	75 kW (105 hp)
Rated speed	2400 rpm
Aspiration	Turbocharged and aftercooled
Injection system	Mechanical direct injection – in-line pump
Oil pan capacity	11.5 qt
Engine length	777 mm
Engine width	625 mm
Engine height	958 mm
Wet weight	340–354 kg

2. OIL PAN CONFIGURATION AND MATERIAL SELECTION

This section outlines the oil pan configuration and the material framework adopted in this study, providing the necessary context to interpret the structural and thermo-mechanical results discussed later. The focus is placed on how component geometry, internal structural features, and material properties interact under service-relevant conditions, rather than on manufacturing or numerical implementation details [15].

The analyzed oil pan corresponds to a representative automotive design incorporating sealing interfaces, mounting regions, and externally reinforced walls that govern stiffness distribution and load transfer. When replacing cast aluminum with a polymer-based solution, these geometric features become critical, as temperature-induced material softening modifies the dominant load paths within the component.

Accordingly, material selection is considered in conjunction with structural configuration. A direct comparison between cast aluminum and recycled glass-fiber-reinforced polyamide (rPA66-GF35) is used to assess whether geometry-driven design strategies can offset the reduced intrinsic stiffness of the polymer while meeting functional and structural requirements.

2.1 Functional requirements of the oil pan under real operating conditions

The oil pan is a multifunctional structural component that operates under a combination of thermal, mechanical, and environmental loading conditions. Unlike purely structural

housings, its performance is governed not only by strength and stiffness requirements, but also by its ability to maintain hermetic sealing, ensure oil flow stability, and withstand accidental external impacts throughout the vehicle's service life. These requirements become particularly critical when conventional metallic materials are replaced by polymer-based solutions, whose mechanical behavior is strongly temperature-dependent.

From a thermal perspective, the oil pan is continuously exposed to elevated lubricant temperatures during sustained engine operation [16]. In the present steady-state thermal analysis, a temperature of 140 °C is prescribed at the internal surfaces of the oil pan to represent a conservative upper-bound operating condition of hot engine oil under prolonged load [17]. At the sealing interface with the engine block, a reduced reference temperature of 100 °C is imposed, reflecting partial heat dissipation through the block and the clamped joint region. Externally, the oil pan is subjected to convective cooling to the surrounding air, which is modeled using an ambient temperature of 22 °C and a uniform convective heat transfer coefficient of 20 $W \cdot m^{-2} \cdot °C^{-1}$, corresponding to natural convection conditions typically assumed for underbody components exposed to airflow without forced cooling [18]. This combination of internal temperature loading and external convective boundary conditions defines the thermal gradients governing the initial deformation state of the oil pan and directly influences stiffness retention and sealing performance. Figure 2 illustrates the thermal exposure zones and service-relevant temperature conditions applied to the oil pan.

In light of these conditions, it is critical to contextualize the 140 °C thermal boundary condition against the 110 °C long-term service temperature limit of the rPA66-GF35 polymer. As noted, the 140 °C internal temperature is a conservative thermal peak to evaluate maximum structural softening. During normal, sustained operation, bulk oil temperatures remain within the material's 110 °C continuous service limit. Most importantly, the convective cooling applied to the exterior establishes a steep thermal gradient across the thickness of the pan. Consequently, the external reinforcement ribs—which act as the primary load-carrying members—operate at steady-state temperatures significantly below the internal 140 °C peak and safely within the operational limits of the polymer, preserving the overall structural stiffness of the component.

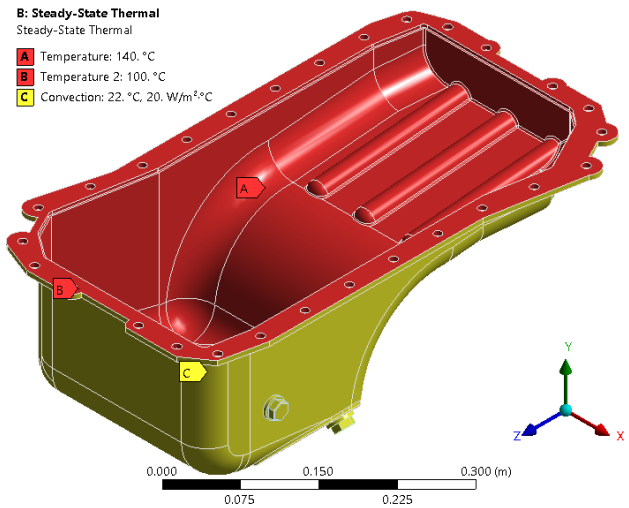

Figure 2. Thermal boundary conditions applied to the oil pan under representative engine operating conditions

At elevated temperatures, polymer-based materials experience a marked reduction in elastic modulus and load-bearing capacity, which affects both global stiffness and localized deformation [19]. This thermal softening is particularly critical at the sealing interface between the oil pan and the engine block, where excessive deformation may compromise gasket compression and lead to oil leakage, even in the absence of high mechanical loads.

Mechanically, the oil pan must withstand static and quasi-static loads arising from the oil mass, mounting constraints, and engine-induced reactions. In addition, dynamic excitations transmitted from the powertrain can amplify local stresses and influence the modal behavior of the component, with direct implications for NVH performance. Internal structural features originally intended for oil flow control also contribute to load transfer and stiffness distribution, reinforcing the coupled nature of functional and structural requirements [20, 21].

Environmental and accidental loading conditions further increase the design complexity. Located at the lowest point of the powertrain assembly, the oil pan is vulnerable to impacts from road debris, speed bumps, and uneven terrain. Under such conditions, localized impact resistance and energy absorption capacity become critical performance indicators, particularly for polymer components, where strain-rate sensitivity and temperature-dependent failure modes must be considered [22].

Table 2 summarizes the primary functional requirements of the oil pan under real operating conditions, emphasizing the need to satisfy multiple performance criteria simultaneously. This highly constrained operational envelope motivates the thermo-structural evaluation and geometry-driven design strategies presented in the subsequent sections.

The combination of these requirements defines a highly constrained design space, where material selection alone is insufficient to guarantee acceptable performance. Instead, the interaction between material behavior, geometry, and externally driven structural reinforcement becomes the dominant factor governing oil pan reliability. This observation motivates the subsequent thermo-structural evaluation and geometry-driven optimization strategies presented in the following sections [23].

Table 2. Functional requirements of the oil pan under real operating conditions

Operating Environment	Dominant Loading Condition	Functional Requirement	Performance Criterion
Thermal	Oil temperature up to 140 °C	Stiffness retention	Limited deformation at the sealing line
Mechanical (static)	Oil mass and mounting loads	Structural integrity	Stress below allowable limits
Mechanical (dynamic)	Engine-induced vibrations	Dynamic stability	Acceptable modal response / NVH
Environmental	Road debris and obstacles	Impact resistance	No cracking or loss of sealing
Functional	Oil motion and sloshing	Flow control	Stable oil distribution

2.2 Structural reinforcement features and load-carrying mechanisms

The structural behavior of the oil pan is strongly influenced by the presence and configuration of reinforcement features that define load-carrying mechanisms under combined thermal and mechanical loading. In polymer-based designs, these features play a more critical role than in metallic counterparts due to the lower elastic modulus and temperature-dependent stiffness degradation [24].

In the reference configuration, internal geometric features originally intended for oil flow control provide secondary load paths and contribute to global stiffness. However, for polymer materials, their continuous exposure to hot lubricating oil reduces their structural effectiveness. To address this limitation, the reinforcement strategy adopted in this study relocates the primary stiffening features to the external surfaces of the oil pan [25].

Externally positioned ribs operate at lower steady-state temperatures due to convective heat transfer, allowing them to retain higher effective stiffness than internally immersed features. Figure 3 illustrates the external rib configuration and the associated load transfer mechanisms under mechanical loading [26]. This geometry-driven approach enables stiffness enhancement without increasing material thickness or mass, making it particularly suitable for polymer oil pan applications.

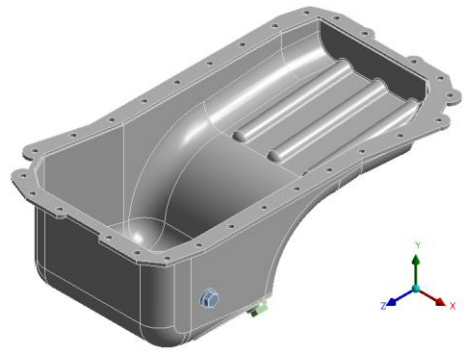

(a) Baseline oil pan geometry

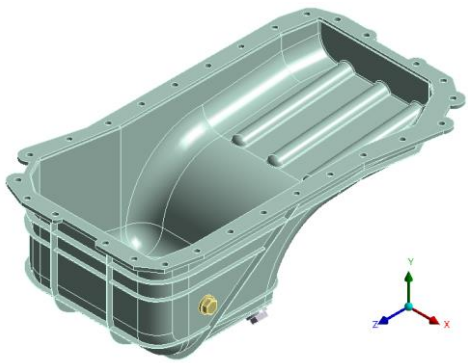

(b) Oil pan geometry with external rib reinforcements

Figure 3. Baseline and externally reinforced oil pan configurations

2.3 Material substitution strategy: Cast aluminum vs. rPA66-GF35

The material substitution strategy evaluated in this work compares a conventional cast aluminum oil pan with a design based on recycled glass-fiber-reinforced polyamide (rPA66-GF35). Cast aluminum is used as a reference due to its high stiffness retention and long-term dimensional stability under engine operating temperatures, while rPA66-GF35 is selected for its low density, reduced environmental impact, and favorable vibration damping behavior [27, 28].

The fundamental challenge associated with rPA66-GF35 is not its room-temperature strength, which is comparable to aluminum in tensile terms, but rather its pronounced stiffness degradation with increasing temperature. Under hot oil exposure, the elastic modulus of polyamide decreases sharply, directly affecting bending stiffness, flange stability, and sealing integrity [29]. For this reason, material substitution in this study is not based on material equivalence, but on functional equivalence, achieved through geometry-driven reinforcement [30].

This contrast between intrinsic material capability and temperature sensitivity is quantified in Table 3, which replaces the qualitative comparison with a set of engineering-relevant properties for both materials.

Table 3. Engineering property comparison between cast aluminum and rPA66-GF35

Property	Cast Aluminum (A356-T6)	rPA66-GF35 (Engineering Datasheet)
Density (kg·m^{-3})	2700	1350–1450
Flexural modulus at 23 °C (MPa)	70 000	10 500–13 500
Tensile strength at 23 °C (MPa)	200	185–220
Impact strength	Moderate	High (80-110 kJ·m^{-2})
Glass transition temperature, Tg (°C)	Not applicable	72–110
Heat deflection temperature (°C)	≫200	120–170
Long-term service temperature (°C)	High	110

While Table 3 shows that rPA66-GF35 offers major advantages in density, impact resistance, and environmental footprint, it also reveals the fundamental limitation of polymer-based oil pans: their stiffness is thermally fragile [31]. This limitation is quantified in Figure 4, which presents the normalized elastic modulus retention $E(T)/E_{23}$ for rPA66-GF35 and aluminum over the service-relevant temperature range.

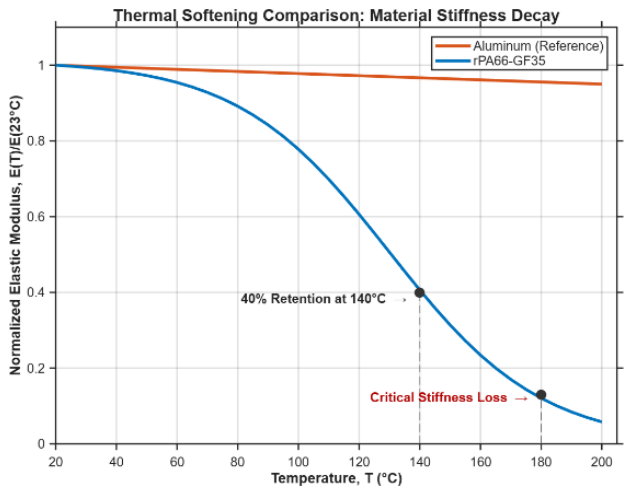

Figure 4. Normalized elastic modulus retention of rPA66-GF35 and cast aluminum as a function of temperature

In cast aluminum, the elastic modulus remains almost constant across the full operating envelope, decreasing by less than 5% between 20 ℃ and 200 ℃. In contrast, rPA66-GF35 exhibits a dramatic reduction, retaining only about 40% of its room-temperature stiffness at 140 ℃ and falling below 20% at 180 ℃. This steep modulus decay explains why polymer oil pans cannot rely on shell thickness or material strength alone to guarantee sealing and dimensional stability [32, 33].

Figure 4, therefore, provides the physical justification for the geometry-driven reinforcement strategy adopted in this work: as material stiffness collapses with temperature, structural integrity must be recovered through increases in geometric inertia and controlled load paths, implemented here through externally reinforced ribs. The thermo-mechanical simulations presented in the following sections directly quantify how this geometric compensation offsets the temperature-induced loss of material stiffness.

3. THERMO-STRUCTURAL RESPONSE AT OPERATING CONDITIONS

The thermo-structural response of the oil pan is a critical performance indicator when polymer-based materials are subjected to engine-relevant operating conditions [34, 35]. Unlike metallic components, whose stiffness remains relatively stable within the temperature range of lubricating oil, glass-fiber-reinforced polymers exhibit a pronounced coupling between thermal exposure and mechanical behavior. As a result, temperature fields directly influence deformation patterns, stress distribution, and sealing-line integrity.

In this study, the thermo-structural response is evaluated under steady-state operating conditions representative of sustained engine operation. The imposed thermal environment reflects the combined effect of hot lubricating oil, engine block contact, and external convective cooling, allowing the structural consequences of temperature-dependent material behavior to be quantified. The analysis focuses on identifying critical regions where thermal softening leads to stiffness loss and increased deformation, particularly in areas governing sealing performance and global structural stability.

Table 4. Finite element analysis (FEA) setup and boundary conditions

Setup Parameter	Configuration Details
Solver environment	ANSYS Mechanical 2025 R2 (Student Version)
Analysis type	Sequential Coupling (Steady-State Thermal > Static Structural)
Element type	3D Higher-order solid elements (e.g., 10-node tetrahedra)
Mesh size	Global element size: 3.0 mm (Unstructured mesh: 170,319 elements; 338,111 nodes)
Contact assumptions	Bonded contact formulation at the engine block interface
Mounting constraints	Fixed supports applied directly to the 28 bolt mounting hole faces
Mechanical loads	Standard earth gravity (9.81 m/s²) applied along the negative vertical axis (-Y)
Oil load representation	Hydrostatic pressure applied to wetted inner walls based on an assumed oil density of 900 kg/m³
Thermal load	Imported 3D temperature field from thermal analysis (Peak temperature: ~140 ℃)

3.1 Finite element model setup

To evaluate the structural integrity and sealing performance under elevated temperatures, a sequential one-way thermo-mechanical coupling was configured. The detailed parameters governing the finite element environment, discretization, and boundary conditions are summarized in Table 4.

3.2 Temperature-dependent stiffness degradation of rPA66-GF35

The mechanical response of rPA66-GF35 is strongly affected by temperature, with a significant reduction in elastic modulus as operating temperatures approach those of the lubricating oil [25]. Under steady-state thermal conditions, this stiffness degradation becomes the dominant factor governing the structural behavior of the oil pan, even in the absence of high external mechanical loads. This thermo-mechanical coupling is governed by the temperature-dependent constitutive law of the polymer, which relates stress and strain through a stiffness tensor that varies with temperature. This relationship is expressed by Eq. (1):

$$\sigma = D(T) : \varepsilon \tag{1}$$

where, σ is the Cauchy stress tensor, ε is the total strain tensor, and $D(T)$ is the temperature-dependent stiffness tensor of rPA66-GF35.

The temperature sensitivity of this tensor is governed primarily by the degradation of the elastic modulus with increasing temperature. This dependence is introduced through Eq. (2):

$$D(T) = D(E(T), \nu) \tag{2}$$

where, $E(T)$ is the elastic modulus of the polymer at temperature T, and ν is Poisson's ratio. As the oil temperature approaches 140 ℃, $E(T)$ decreases significantly, reducing the effective stiffness of the oil pan even under moderate mechanical loading.

Figure 5 shows the steady-state temperature distribution within the oil pan under operating conditions, highlighting the elevated temperatures at the internal surfaces in contact with the oil and the lower temperatures at the externally cooled regions. The resulting thermal gradients generate spatially non-uniform stiffness degradation, as predicted by Eqs. (1) and (2), leading to localized compliance in the hottest regions.

As temperature increases, the reduced modulus $E(T)$ amplifies both global and local deformation under self-weight, oil mass, and mounting constraints. This effect is particularly evident near the sealing interface and the base plate, where stiffness loss can translate directly into increased displacement and potential loss of gasket compression. Figure 6 presents the imported body temperature field applied to the structural model, which serves as the thermal input for the coupled thermo-structural analysis.

In addition to stiffness degradation, the thermal field introduces direct thermal strains in the constrained polymer structure [36]. These thermally induced strains are defined by Eq. (3):

$$\varepsilon_{th} = \alpha(T - T_0)I \tag{3}$$

where, α is the coefficient of thermal expansion, T_0 is the stress-free reference temperature, and I is the identity tensor. Eq. (3) shows that even in the absence of external forces, the temperature field in Figure 6 generates internal strains that interact with mechanical constraints and stiffness degradation to produce the deformation patterns observed in the oil pan.

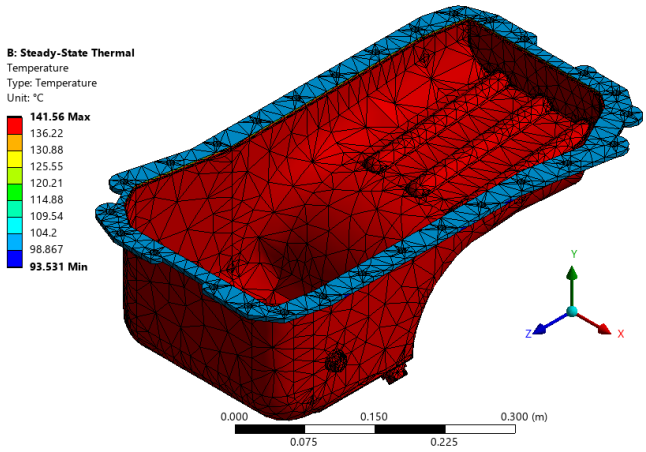

Figure 5. Steady-state temperature distribution in the oil pan under operating conditions

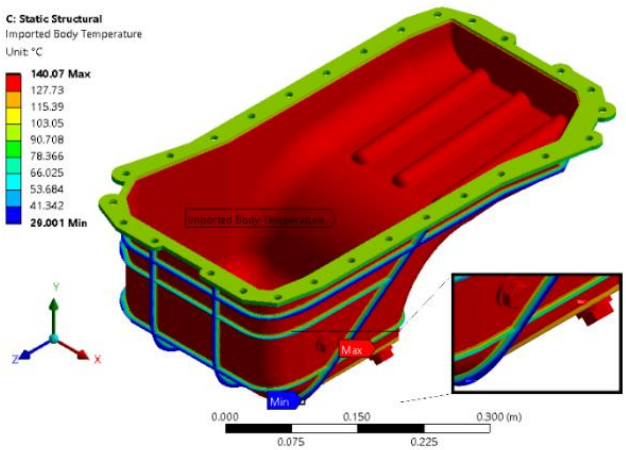

Figure 6. Imported body temperature

The influence of temperature-dependent stiffness and thermally induced strain is further reflected in the strain response of the oil pan. Elevated elastic strains develop in regions combining high temperature exposure and structural constraint, indicating zones where material softening and thermal expansion interact. Figure 7 illustrates the equivalent elastic strain distribution obtained from the thermo-structural analysis, emphasizing the sensitivity of the polymer material to the coupled mechanisms described by Eqs. (1)-(3).

These results confirm that, for rPA66-GF35 oil pans, structural performance cannot be assessed independently of thermal conditions. Instead, stiffness degradation and thermally induced strain, as formalized by Eqs. (1)-(3) and imposed through the temperature fields in Figures 5 and 6, govern the deformation and sealing-relevant response, motivating the geometry-driven reinforcement strategies evaluated in the subsequent sections.

3.3 Thermo-mechanical deformation and stress response

The global deformation and stress response of the oil pan under combined thermal and mechanical loading provides a direct measure of structural adequacy for polymer-based designs. In the present analysis, the applied loads include the steady-state thermal field, the oil mass, mounting constraints, and gravity, representing a realistic service condition for the Cummins 4BT 3.9 engine.

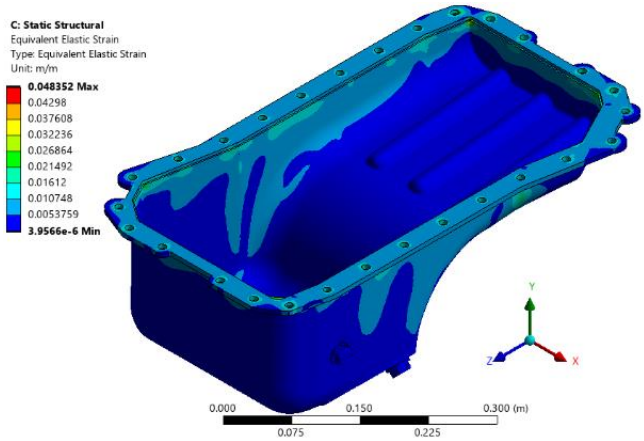

(a) Baseline oil pan – equivalent elastic strain

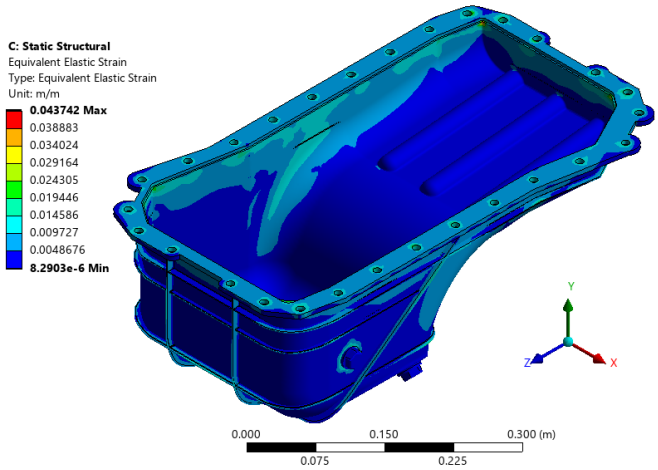

(b) Externally reinforced oil pan – equivalent elastic strain

Figure 7. Equivalent elastic strain distribution before and after external rib reinforcement

Under these conditions, deformation is governed by the combined action of mechanically induced strain and thermally induced strain. This coupling is formally described by the total strain decomposition given in Eq. (4):

$$\varepsilon = \varepsilon_{mech} + \varepsilon_{th} \tag{4}$$

where, ε_{mech} represents the strain generated by oil mass, gravity, and mounting constraints, and ε_{th} is the thermal strain induced by the temperature field imported from the steady-state thermal analysis.

The corresponding stress field follows from the temperature-dependent constitutive behavior of rPA66-GF35. The thermo-elastic stress–strain relation is given by Eq. (5):

$$\sigma = D(T) : (\varepsilon_{mech} + \varepsilon_{th}) \tag{5}$$

where, $D(T)$ is the elastic stiffness matrix of the polymer evaluated at the local operating temperature. This equation

explains why thermal softening leads to increased deformation and stress redistribution even when the applied mechanical loads remain unchanged.

Figure 8 compares the total deformation of the baseline oil pan geometry and the externally reinforced configuration. In the baseline design, stiffness degradation at elevated temperatures leads to increased global deformation, particularly in the base plate and regions distant from the mounting interfaces. The introduction of external rib reinforcements significantly alters the deformation pattern by increasing bending stiffness and redirecting loads toward structurally favorable regions.

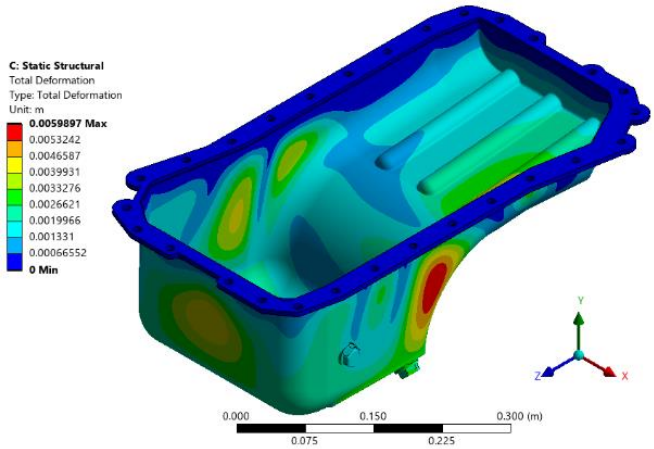

(a) Baseline geometry

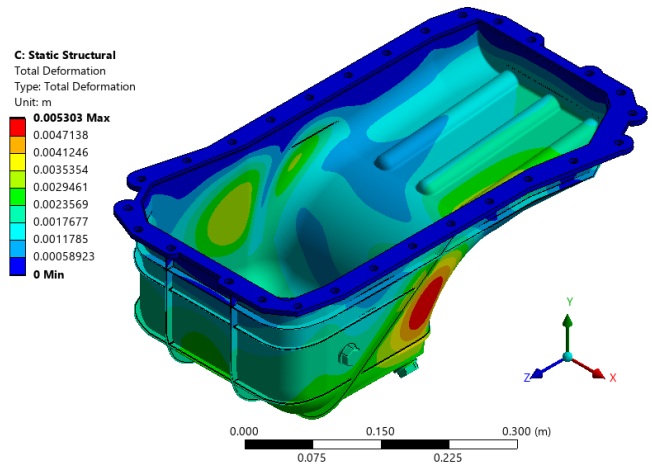

(b) Externally reinforced configuration

Figure 8. Total deformation of the oil pan under combined thermo-mechanical loading

To assess the multiaxial stress state associated with these deformation fields, the equivalent von Mises stress is adopted as the governing failure metric [37]. This scalar stress measure is defined by Eq. (6):

$$\sigma_{Von\,Mises} = \sqrt{\frac{(\sigma_1 - \sigma_2) + (\sigma_2 - \sigma_3) + (\sigma_3 - \sigma_1)}{2}} \tag{6}$$

where, σ_1, σ_2, and σ_3 are the principal stresses. This definition establishes the physical meaning of the stress contours presented in Figure 9.

A similar trend is observed in the stress response. Figure 9 presents the equivalent von Mises stress distribution for both configurations under combined loading. While the baseline oil pan exhibits localized stress concentrations near the sealing interface and mounting regions, the reinforced design shows a more uniform stress distribution, with peak stresses shifted away from critical sealing zones and into the rib network. This redistribution indicates improved load-carrying efficiency without an increase in material thickness.

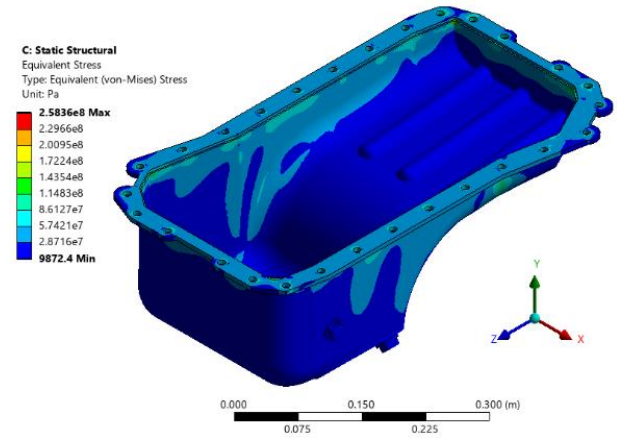

(a) Baseline geometry

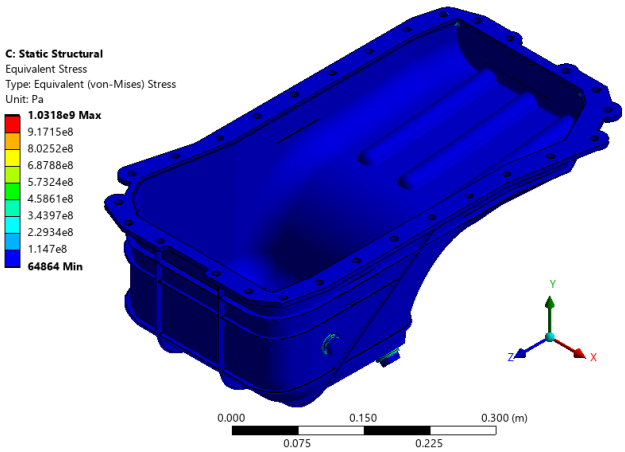

(b) Externally reinforced configuration

Figure 9. Equivalent von Mises stress distribution under combined thermo-mechanical loading

Based on Eqs. (4)–(6), characteristic deformation and stress values were extracted directly from the thermo-mechanical solution fields to provide a quantitative comparison between the two configurations. The resulting numerical data, reported in Table 4, allow the structural response of the baseline and reinforced oil pans to be evaluated in terms of global deformation, mid-section compliance, and stress redistribution under operating temperature and mechanical loading.

The data in Table 5 confirms that the externally reinforced configuration achieves a meaningful reduction in global deformation despite the strong thermal softening of rPA66-GF35 at 140 °C. In particular, the dominant mid-section deformation closely associated with sealing-line stability decreases by approximately 11.5%, indicating improved stiffness retention in the most critical region of the oil pan.

At the same time, the increase in peak von Mises stress observed in the reinforced design reflects a deliberate concentration of load within the rib structures. This behavior is structurally favorable, as it indicates that the added ribs are effectively acting as primary load-carrying members, relieving

the main shell from excessive bending and limiting deformation in sealing-relevant areas. Such stress redistribution is a characteristic and desirable outcome of geometry-driven reinforcement in polymer components operating under high thermal loads.

Table 5. Thermo-mechanical deformation and stress comparison between baseline and externally reinforced oil pan

Parameter	Baseline Oil Pan	Externally Reinforced Oil Pan	Change
Maximum total deformation (m)	0.0059897	0.005303	-11.5%
Dominant deformation zone	Mid-section = 0.0019966 m	Mid-section = 0.0017677 m	Reduced deformation in the sealing-relevant region
Maximum von Mises stress (Pa)	2.5836×10^8	1.0318×10^9	Local stress concentration due to rib load transfer
Typical stress level in sealing and upper region (Pa)	8.61×10^7	$1 – 2 \times 10^8$	Load redistributed to reinforcements
Stress field distribution	Mixed green–blue across the body	Predominantly blue, localized green near bolts	More stable global stress field

3.4 Sealing-line integrity at elevated oil temperatures

Sealing performance is controlled by the ability of the oil pan flange to remain geometrically stable under combined thermo-mechanical loading. In the baseline configuration, the deformation field in Figure 8 shows that global shell bending is directly transmitted to the flange, producing non-uniform out-of-plane displacement and localized loss of gasket compression. This behavior is confirmed by the stress concentrations near the sealing region in Figure 9.

The externally reinforced design alters this load path. The rib network increases bending stiffness and redirects thermo-mechanical loads away from the shell toward the reinforcements, reducing mid-section and flange compliance as quantified in Table 4. As a result, flange deformation is decoupled from global shell bending, preserving sealing geometry even under thermal softening.

Although peak stresses increase, they are concentrated in the ribs rather than in the sealing interface, indicating a controlled and mechanically favorable load transfer. This demonstrates that sealing integrity in polymer oil pans is governed primarily by structural geometry rather than material limitations.

4. GEOMETRY-DRIVEN STIFFNESS RECOVERY

The externally reinforced oil pan demonstrates that stiffness loss induced by the thermal softening of rPA66-GF35 can be effectively compensated through geometric design rather than through material substitution. Under combined thermal and mechanical loading, the baseline oil pan behaves as a thin shell, where bending deformations dominate and are directly transmitted into the sealing and mid-section regions. In contrast, the reinforced configuration introduces a three-dimensional rib network that provides preferential load paths, redirecting bending and shear forces away from the shell and into geometrically efficient structural members.

This behavior is evidenced by the redistribution of von Mises stresses observed in Figure 9 and by the reduction of mid-section deformation reported in Table 4. While the baseline geometry exhibits bending-dominated deformation of the shell, the rib-reinforced configuration transfers a significant fraction of the load into the external ribs and bolt-adjacent regions, thereby stabilizing the main body and preserving sealing-relevant geometry. The increase in local stresses within the ribs is therefore not a structural penalty but an intended outcome of load-path control.

The stiffness recovery produced by this geometric strategy can be interpreted through the bending stiffness of the structure, which depends on both the temperature-dependent elastic modulus of the polymer and the geometric inertia of the cross-section. This relationship is summarized by Eq. (7):

$$k_b \propto E(T) I_p \tag{7}$$

where, $E(T)$ is the elastic modulus of rPA66-GF35 at operating temperature and I_p is the polar moment of inertia reported in Table 5. Since thermal exposure reduces $E(T)$, the only available mechanism to preserve stiffness is an increase in I_p through geometry.

Table 6. Mass and stiffness-relevant geometric properties of baseline and externally reinforced oil pans

Parameter	Baseline Oil Pan	Externally Reinforced Oil Pan	Change
Body volume (m^3)	8.641×10^{-4}	8.998×10^{-4}	+4.13%
Integrated volume from results (m^3)	8.8245×10^{-4}	9.1954×10^{-4}	+4.20%
Mass (kg)	1.062	1.1058	+4.12%
Centroid Z (m)	1.3252	1.3288	+0.27%
Polar inertia Ip1 ($kg \cdot m^2$)	3.6446×10^{-2}	3.7969×10^{-2}	+4.18%
Polar inertia Ip2 ($kg \cdot m^2$)	4.4211×10^{-2}	4.6147×10^{-2}	+4.38%
Polar inertia Ip3 ($kg \cdot m^2$)	1.5123×10^{-2}	1.5736×10^{-2}	+4.05%

Table 6 shows that the introduction of external ribs increases the total polymer volume and mass by only about 4%, while producing a comparable increase in all three principal polar moments of inertia.

This proportional growth explains why the reinforced oil pan achieves a measurable reduction in global and mid-section deformation despite operating under the same degraded material stiffness, as quantified in Table 4.

The spatial distribution of the added material is illustrated in Figure 10, which confirms that the volume increase is concentrated almost exclusively in the lateral external ribs and structural frames, where bending moments are highest. Low-stress regions of the shell remain largely unchanged, which explains why a small mass penalty yields a disproportionately large stiffness recovery. This geometry-driven strategy, therefore, provides an efficient and sustainable pathway for

restoring structural performance in polymer oil pans operating under thermo-mechanical service conditions.

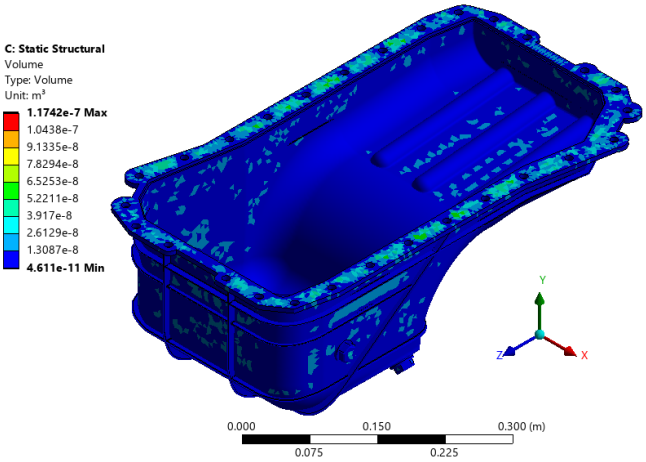

Figure 10. Spatial distribution of added polymer volume in the externally reinforced oil pan

5. ASSESSMENT OF THE OPTIMIZED DESIGN

The preceding sections established, through coupled thermo-mechanical simulation, that external rib reinforcement substantially modifies the load-carrying behavior of the rPA66-GF35 oil pan. However, numerical fields of stress and deformation alone do not guarantee that a design is suitable for real service conditions. This section, therefore, evaluates the expected performance of the optimized geometry in terms of structural adequacy, dynamic robustness, and impact resistance, using the extracted steady-state thermo-mechanical results as engineering performance indicators. It is important to note that while explicit physical validation and transient dynamic simulations of impact and NVH fall outside the scope of this steady-state study, the structural improvements achieved provide a robust theoretical foundation for enhanced dynamic performance. The objective is to assess whether the reinforced configuration theoretically satisfies the functional requirements summarized in Table 2 under representative operating conditions.

5.1 Structural adequacy under service loads

Under sustained engine operation, the oil pan is subjected to a combination of gravity loads from the oil mass, bolt preload at the flange, and thermally induced softening caused by oil temperatures approaching 140 °C [38]. In polymer components, this loading combination is critical because even moderate stresses can lead to excessive deformation if stiffness is insufficient. The reinforced oil pan demonstrates structural adequacy primarily through deformation control rather than stress minimization. As shown by the thermo-mechanical extraction summarized in Table 4, the introduction of external ribs reduces the dominant mid-section deformation by approximately 11.5%, directly improving sealing-line stability and base-plate flatness. This reduction is achieved despite the strong temperature-dependent modulus degradation of rPA66-GF35.

Although the reinforced design exhibits higher local von Mises stresses within the rib network, this behavior is mechanically favorable. These localized stress peaks indicate that the ribs are functioning as intended load-bearing members.

To reinforce this assessment, a design compliance matrix is presented in Table 7, summarizing the primary engineering indicators extracted from the thermo-mechanical analysis. This comparison highlights the structural adequacy of the optimized configuration under the prescribed service loads.

Table 7. Service-load structural adequacy indicators

Indicator	Baseline	Reinforced	Assessment
Max total deformation	0.00599 m	0.00530 m	Improved
Mid-section deformation	0.001997 m	0.001768 m	Improved
Load-bearing mechanism	Shell bending	Rib-dominated	Favorable

Notes: This table functions as a design compliance matrix, which is typical in engineering validation sections.

5.2 Dynamic robustness and noise, vibration, and harshness-relevant behavior

The dynamic robustness of an oil pan is governed primarily by its global stiffness and inertial properties, which control its susceptibility to vibration, resonance, and structure-borne noise transmission from the engine block. For polymer components, this aspect is particularly important because reduced stiffness can shift natural frequencies into the excitation range of the powertrain.

Although a full modal analysis was not required for this study, the geometric and inertial changes introduced by the external ribs provide direct insight into dynamic behavior. As shown in Table 5, the reinforced oil pan exhibits an increase of approximately 4–4.5% in all three polar moments of inertia, accompanied by a comparable increase in mass. This proportional rise indicates that the added material is placed in structurally efficient locations, increasing bending and torsional resistance without excessive weight penalty.

Higher polar inertia and reduced global deformation imply: (i) increased natural frequencies, (ii) reduced vibration amplitudes, (iii) improved resistance to engine-induced excitation.

5.3 Resistance to impact and bottoming loads

In real service, the oil pan is the lowest structural component of the powertrain and is therefore exposed to impacts from road debris, speed bumps, and uneven pavement. For polymer oil pans, resistance to bottoming and impact is governed primarily by geometric stiffness and load-spreading capability rather than by material strength alone.

The externally reinforced configuration improves this behavior by converting the base plate from a bending-dominated shell into a rib-stabilized structural plate. The external ribs distribute localized contact forces over a wider area, reducing peak bending strains and limiting the risk of localized collapse.

This improvement is consistent with the reduced global deformation reported in Table 4, the increased polar moments of inertia in Table 5, and the concentration of added material in the lateral rib network shown in Figure 10. Together, these features indicate that the reinforced oil pan provides higher resistance to bottoming, lower permanent deformation after impact, and improved durability under rough-road operating conditions.

6. ENGINEERING INTERPRETATION

6.1 Geometry as a compensation mechanism for thermal softening

The structural response of the polymer oil pan is governed by its ability to transform membrane and bending loads into axial forces carried by stiffened features. In the baseline geometry, the thin shell is forced to sustain bending moments directly, which produces elevated equivalent stresses in the mid-section and in the sealing flange.

The reinforced configuration modifies this behavior by introducing external ribs that increase the second moment of area and create alternate force paths. As a result, bending moments are converted into axial and shear forces within the rib network, reducing the stress level in the main shell and in the sealing-critical regions. This transformation can be expressed in terms of the factor of safety (FoS) [39], which is defined in Eq. (8) as:

$$FoS = \frac{\sigma_{allow}(T)}{\sigma_{shell}} \tag{8}$$

where, $\sigma_{allow}(T)$ is the temperature-dependent allowable stress of rPA66-GF35, and σ_{shell} is the von Mises stress acting in the oil-pan shell that governs sealing performance.

The values reported in Table 8 demonstrate that while the baseline configuration operates well beyond its admissible limits, the externally reinforced design achieves a structurally sound operating regime. For sealing integrity, this condition is formalized by Eq. (9):

$$FoS \geq 1 \Rightarrow Sealing\ integrity\ \ preserved \tag{9}$$

which provides a direct engineering criterion linking thermo-mechanical stresses to functional leakage risk.

Table 8. Factor of safety (FoS) and critical stress comparison under steady-state thermal conditions

Parameter	Baseline Oil Pan	Externally Reinforced Oil Pan
Allowable stress at 140 °C (MPa)	40	40
Typical von Mises stress in shell (MPa)	86	29.6
Local peak stress (MPa)	110 (localized)	55 (localized in ribs)
Governing stress for sealing integrity	Shell stress	Shell stress
Factor of safety (FoS) ($FoS = \sigma_{allow}/\sigma_{shell}$)	0.47	1.35
Sealing-line structural margin	Failing	Structurally Adequate

Note: Peak stress values in ribs are associated with localized numerical singularities at the constraint points and do not represent the generalized stress state of the reinforcement network.

6.2 External ribbing as a load-path control strategy

The stress patterns obtained in Section 3 confirm that the ribs act as primary load-carrying members rather than passive stiffeners. In the reinforced configuration, moderate stress concentrations (up to 55 MPa) are confined to the rib network and fastener interfaces, while the main shell remains in a low-stress state below the 40 MPa threshold. This redistribution is reflected in the safety-factor fields shown in Figure 11, where the baseline design exhibits extended regions operating in a failure state (FoS < 1), whereas the reinforced geometry confines the lowest safety factors to the structural ribs. This confirms that the rib layout enforces a controlled load path, redirecting global bending and shear loads away from the shell and into geometrically efficient members. The increase in polar moments of inertia documented in Table 5 supports this interpretation, indicating a higher resistance to both bending and torsional deformation. Therefore, the factor-of-safety values represent a structural improvement driven by load-path reconfiguration rather than a change in intrinsic material properties.

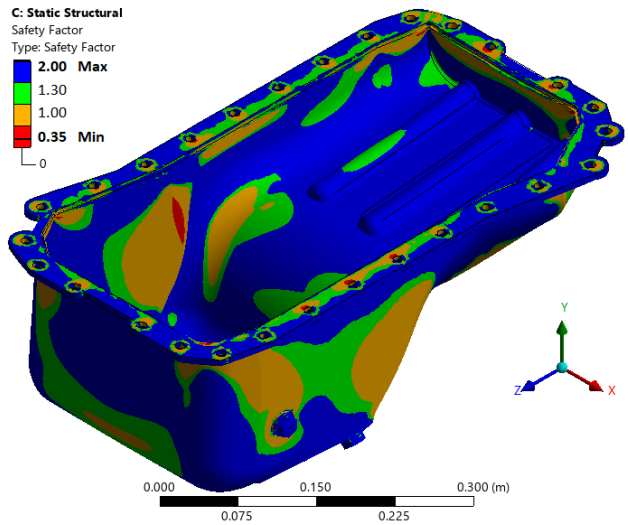

(a) Baseline geometry

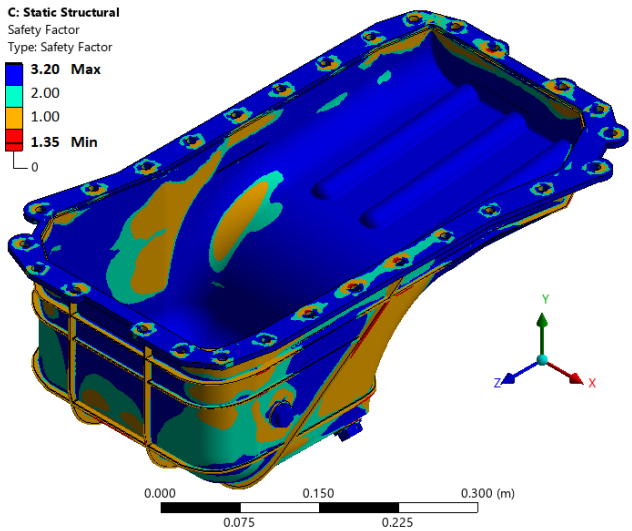

(b) Externally reinforced configuration

Figure 11. Minimum factor-of-safety distribution for the baseline and externally reinforced oil pan under combined thermo-mechanical service loads

6.3 Design trade-offs and scope of applicability

The reinforced design achieves structural admissibility with a mass increase of approximately 4%, which is mechanically efficient for a polymer-based component. As shown by the factor-of-safety comparison in Table 7, this modest material addition is sufficient to shift the oil pan from an overstressed

condition to a stable operating regime.

This approach is particularly suitable for oil pans and similar housings governed by bending-dominated behavior affecting sealing and flange stability. The concept remains valid as long as loads can be redirected into rib-supported load paths. Applications dominated by severe impact or localized crushing would require additional local reinforcement, but under service loading conditions typical of engine oil pans, the present geometry provides a structurally sound and lightweight solution.

While the reinforced design achieves structural admissibility under steady-state conditions, certain limitations must be acknowledged. This study focuses on the immediate thermo-mechanical response; however, long-term degradation mechanisms such as creep and fatigue under cyclic thermal loading remain outside the current scope. Additionally, while the increased stiffness implies improved dynamic behavior, applications subject to severe high-velocity impacts or localized crushing would require further dynamic characterization. The current geometry provides a structurally sound and lightweight solution specifically for service loading conditions typical of diesel engine oil pans

Table 9. Comparative thermo-mechanical performance between the optimized polymer and the reference aluminum oil pan

Performance Metric	Optimized Polymer (rPA66-GF35)	Cast Aluminum (Reference A356-T6)	Variation (Polymer vs. Al)
Mass (kg)	1.106	1.837	- 39.8%
Max. total deformation (mm)	5.30	0.68	+ 679%
Sealing-line deformation (mm)	1.77	0.178	+ 894%
Typical shell stress (MPa)	29.6	49.6	- 40.3%
Factor of safety (FoS)	1.35	~ 5.0	-

Note: Peak localized stresses occurring strictly at the idealized rigid boundary constraints were identified as numerical singularities and excluded from the typical shell stress evaluation to represent realistic operating states.

6.4 Comparative benchmarking against cast aluminum

To rigorously address the structural viability of the proposed rPA66-GF35 geometry, a direct comparative analysis was conducted against a baseline aluminum (A356-T6) oil pan of equivalent 3.0 mm shell thickness under identical thermo-mechanical loading (140 °C). As detailed in Table 9, the aluminum reference exhibits a highly rigid response, with a maximum global deformation of only 0.68 mm and a near-zero sealing-line deformation of 0.178 mm. However, this rigidity comes at a significant mass penalty, yielding a total component weight of 1.837 kg. In contrast, the topology-optimized polymer design achieves a structurally sound sealing-line deformation (1.77 mm) that falls within acceptable gasket compression tolerances, while maintaining typical shell stresses well below its temperature-degraded allowable limits (~29.6 MPa). Most importantly, this is achieved while reducing the overall mass to 1.106 kg—a nearly 40% weight reduction. Although the absolute deformation of the polymer is inherently higher due to its lower elastic modulus, the geometry-driven load paths successfully decouple this compliance from the critical sealing interface. This validates the optimized polymer configuration as a sustainable, lightweight alternative that meets the functional threshold requirements without the mass burden of conventional metallic housings.

7. CONCLUSIONS

This study demonstrates that a polymer oil pan manufactured from rPA66-GF35 can successfully replace a cast-aluminum component only when geometry is deliberately engineered as a stiffness-restoration mechanism rather than as a simple shell.

The baseline polymer geometry, although lightweight and thermally resistant, exhibits bending-dominated behavior that compromises structural stability and sealing reliability under service loading. The present case study indicates that such failure is not strictly a material limitation, but strongly dependent on geometric configuration. By introducing externally driven rib networks that act as primary load paths, the reinforced design converts a flexible shell into a controlled structural system. The engineering effectiveness of this strategy is evidenced by a significant shift from a critical failure state (FoS = 0.47) to a safe operating regime (FoS = 1.35), effectively reducing typical shell stresses from 86 MPa to 29.6 MPa. Furthermore, the geometric efficiency of the design is highlighted by the fact that a marginal mass increase of only 4.12 yielded a proportional increase in polar moments of inertia, achieving a 11.5% reduction in critical mid-section deformation. Consequently, the component is transformed from a compliant housing into a rib-stabilized structural enclosure, ensuring sealing integrity even under the severe thermal conditions of 140 °C. The engineering implication for the analyzed Cummins 4BT 3.9 engine platform is clear: lightweight polymer oil pans become structurally viable in high-temperature environments when topology and external reinforcement are explicitly designed to compensate for thermally induced modulus loss.

A direct comparative benchmarking against a cast aluminum (A356-T6) oil pan reveals that, although the metallic component offers superior absolute rigidity (0.178 mm of sealing-line deformation), the optimized rPA66-GF35 polymer design safely maintains sealing integrity (1.77 mm) while achieving a 40% reduction in mass (1.106 kg versus 1.837 kg). By effectively transferring loads through the external rib network rather than the primary shell, the polymer configuration achieves a highly competitive mass-normalized stiffness. This validates the optimized design as a sustainable, high-performance alternative to conventional metallic housings for diesel engines such as the Cummins 4BT 3.9.

It is important to acknowledge that this study focuses on the steady-state thermo-mechanical response; factors such as long-term creep, cyclic thermal fatigue, and high-velocity impact resistance were not modeled and represent critical areas for future investigation.

ACKNOWLEDGMENT

We thank the Universidad Nacional de San Agustín de Arequipa for their support and knowledge.

REFERENCES

[1] Hohenstein, T., Gleiter, U., Glaser, S., Fritz, T. (2010). First volume application of impact-resistant plastic oil pans. MTZ Worldwide, 71(1): 28-34. https://doi.org/10.1007/BF03226999

[2] Zouani, A., Smith, T., Valencia, F., Gan, C., Sabharwal, M., Lee, C., Bhosale, A., Kondapalli, P. (2009). NVH development of lightweight polymer engines oil pans for gasoline. In SAE 2009 Noise and Vibration Conference and Exhibition. SAE Technical Paper. https://doi.org/10.4271/2009-01-2060

[3] Barton, D.C., Fieldhouse, J.D. (2018). Automotive Chassis Engineering. Berlin: Springer, p. 337. https://doi.org/10.1007/978-3-031-57526-6_6

[4] Zhang, W., Xu, J. (2022). Advanced lightweight materials for Automobiles: A review. Materials & Design, 221: 110994. https://doi.org/10.1016/j.matdes.2022.110994

[5] Yurdakul, M., Tok, M., Döner, G.S., Kırbıyık Kurukavak, Ç. (2026). Sustainable Polymer Composites for Automotive Industry. In Macro, Micro and Nanocomposites from Sustainable Sources: Shrinking Environmental Footprints, Singapore: Springer Nature Singapore, pp. 151-173. https://doi.org/10.1007/978-981-95-2469-3_6

[6] Volpe, V., Lanzillo, S., Affinita, G., Villacci, B., Macchiarolo, I., Pantani, R. (2019). Lightweight high-performance polymer composite for automotive applications. Polymers, 11(2): 326. https://doi.org/10.3390/polym11020326

[7] Mouti, Z., Westwood, K., Kayvantash, K., Njuguna, J. (2010). Low velocity impact behavior of glass filled fiber-reinforced thermoplastic engine components. Materials, 3(4): 2463-2473. https://doi.org/10.3390/ma3042463

[8] Mudhukrishnan, M., Hariharan, P., Palanikumar, K. (2020). Measurement and analysis of thrust force and delamination in drilling glass fiber reinforced polypropylene composites using different drills. Measurement, 149: 106973. https://doi.org/10.1016/j.measurement.2019.106973

[9] Heywood, J.B. (2018). Internal Combustion Engine Fundamentals. 2nd Edition. New York, USA: McGraw-Hill Education.

[10] Glaser, S., Jakobi, R., Kraft, W.W., Wüst, A. (2009). Simulation, production, testing complete package for plastic component development. ATZ Worldwide, 111(5): 36-41. https://doi.org/10.1007/BF03225072

[11] Ma, Q., Wang, S., Zhou, Q., Gan, X. (2021). Parallel optimization of design and manufacture for carbon fiber reinforced plastic oil pan based on the thickness distribution. Polymer Composites, 42(12): 6648-6663. https://doi.org/10.1002/pc.26329

[12] Singh, M.M., Kumar, H., Kumar, G.H., Sivaiah, P., Nagesha, K.V., Ajay, K.M., Vijaya, G. (2020). Determination of strength parameters of glass fibers reinforced composites for engineering applications. Silicon, 12(1): 1-11. https://doi.org/10.1007/s12633-019-0078-3

[13] Cummins Inc. Cummins Official Website. (2023). Cummins 4BT 3.9 Engine Specifications. https://www.cummins.com, accessed on Jan. 13, 2026.

[14] Stone R. (2017). Introduction to Internal Combustion Engines. 4th Edition. London, United Kingdom: Bloomsbury Publishing. https://doi.org/10.1007/978-1-349-14916-2

[15] Panza, M.A. (2015). A review of experimental techniques for NVH analysis on a commercial vehicle. Energy Procedia, 82: 1017-1023. https://doi.org/10.1016/j.egypro.2015.11.861

[16] Lakshminarayanan, P.A., Agarwal, A.K. (2022). Handbook of Thermal Management of Engines. Springer Singapore. https://doi.org/10.1007/978-981-16-8570-5

[17] Bergman, T.L., Lavine, A.S., Incropera, F.P., DeWitt, D.P. (2017). Fundamentals of Heat and Mass Transfer. 8th Edition. Hoboken, New Jersey: John Wiley & Sons.

[18] Bird, R.B., Stewart, W.E., Lightfoot, E.N. (2007). Transport Phenomena. 2nd Edition. New York: John Wiley & Sons.

[19] Vadivelu, M.A., Kumar, C.R., Joshi, G.M. (2016). Polymer composites for thermal management: A review. Composite Interfaces, 23(9): 847-872. https://doi.org/10.1080/09276440.2016.1176853

[20] Müller, J., Jacobs, G., Ramm, M., Wischmann, S., Jagla, P., Berroth, J. (2023). Model-based NVH optimization of a tractor drivetrain during different phases of a design adaption. Forschung im Ingenieurwesen, 87(1): 363-373. https://doi.org/10.1007/s10010-023-00632-3

[21] Antonioli, P., Ruotolo, R., Rimondi, M., Lomario, D. (2011). CAE-based approach for oil pan NVH optimization of compact automotive diesel engines. SAE Technical Paper (No. 2011-01-0934). https://doi.org/10.4271/2011-01-0934

[22] Dong, Y., Du, C., Wang, X., Fan, Y., Liao, S., Han, Y. (2025). Research on the influence of plastic oil pan of the engine on the NVH performance. In 2024 3rd International Conference on Energy and Power Engineering (EPE-AEIC 2024), Lanzhou, China, p. 012033. https://doi.org/10.1088/1742-6596/2932/1/012033

[23] Huang, K., Li, Z., Yang, S. (2026). A modal performance-driven topology optimization framework for structural vibration avoidance. Engineering Structures, 352: 122094. https://doi.org/10.1016/j.engstruct.2026.122094

[24] Osman, A. (2014). Design and development of a compact and lightweight oil pan for high performance vehicle applications. In SAE 2014 World Congress & Exhibition. SAE Technical Paper, 1-12. https://doi.org/10.4271/2014-01-1640

[25] Zhu, X., Zhong, C., Zhe, J. (2017). Lubricating oil conditioning sensors for online machine health monitoring–A review. Tribology International, 109: 473-484. https://doi.org/10.1016/j.triboint.2017.01.015

[26] Aljaghtham, M., Celik, E. (2020). Design optimization of oil pan thermoelectric generator to recover waste heat from internal combustion engines. Energy, 200: 117547. https://doi.org/10.1016/j.energy.2020.117547

[27] Gkaliou, K., Ørsnæs, M.V., Holm, A.H., Daugaard, A.E. (2025). Accelerated hydrolytic degradation of glass fiber-polyamide (PA66) composites. Polymer Degradation and Stability, 234: 111256. https://doi.org/10.1016/j.polymdegradstab.2025.111256

[28] Geretschläger, K.J., Wallner, G.M. (2018). Aging characteristics of glass fiber-reinforced polyamide in hot water and air. Polymer Composites, 39(4): 997-1005. https://doi.org/10.1002/pc.24070

[29] Nikforooz, M., Montesano, J., Golzar, M., Shokrieh, M.M. (2018). Fatigue behavior of laminated glass fiber reinforced polyamide. Procedia Engineering, 213: 816-823. https://doi.org/10.1016/j.proeng.2018.02.077
[30] Hussain, A.R.J., Alahyari, A.A., Eastman, S.A., Thibaud-Erkey, C., Johnston, S., Sobkowicz, M.J. (2017). Review of polymers for heat exchanger applications: Factors concerning thermal conductivity. Applied Thermal Engineering, 113: 1118-1127. https://doi.org/10.1016/j.applthermaleng.2016.11.041
[31] Salvi, A., Marzullo, F., Ostrowska, M., Dotelli, G. (2025). Thermal degradation of glass fibre-reinforced polyamide 6, 6 composites: Investigation by accelerated thermal ageing. Polymers, 17(4): 509. https://doi.org/10.3390/polym17040509
[32] Whitfield, T., Kuboki, T., Wood, J., Ugresic, V., Sathyanarayana, S., Dagnon, K. (2018). Thermal properties of glass fiber reinforced polyamide 6 composites throughout the direct long-fiber reinforced thermoplastic process. Polymer Engineering & Science, 58(1): 46-54. https://doi.org/10.1002/pen.24529
[33] Blaznov, A.N., Samoilenko, V.V., Zimin, D.E., Komarova, M.V., Ananieva, E.S., Firsov, V.V., Sakoshev, Z.G. (2021). Heat-resistance enhancement of fiberglass-reinforced plastics in manufacturing environments. Glass and Ceramics, 78(3): 111-114. https://doi.org/10.1007/s10717-021-00357-1
[34] Ma, Q., Wang, S., Zhou, Q., Gan, X. (2021). Parallel optimization of design and manufacture for carbon fiber reinforced plastic oil pan based on the thickness distribution. Polymer Composites, 42(12): 6648-6663. https://doi.org/10.1002/pc.26329
[35] Guan, Y., Cheng, F., Pan, Z. (2019). Superwetting polymeric three dimensional (3D) porous materials for oil/water separation: A review. Polymers, 11(5): 806. https://doi.org/10.3390/polym11050806
[36] Ttito, D.N., Suarez, D.Q., Gutierrez, J.A., Quispe, W.B., Carpio, P.P., Arapa, C.D. (2025). Design and implementation of fog light ducts to optimize hot air recirculation and heat transfer in the Toyota Hilux. International Journal of Heat and Technology, 43(5): 1631-1643. https://doi.org/10.18280/ijht.430502
[37] Guzman, C.D.S., Jacinto, E.E.C., Vidal, Y.L.S., Quispe, W.F.B., Arapa, C.A.D. (2025). Structural and dynamic performance of a street sweeper chassis with diagonal suspension subjected to standard speed bumps. Advances in Science and Technology Research Journal, 19(12): 138-155. https://doi.org/10.12913/22998624/209886
[38] Kartal, Y., Isin, O. (2019). Numerical investigation on oil pan design parameters to improve engine performance during oil cool down and warm up periods. International Journal of Automotive Technology, 20(3): 465-475. https://doi.org/10.1007/s12239-019-0044-5
[39] Macedo, J., Molina, J., Vidal, Y.S., Mendoza, A., Canazas, J., Diaz, C. (2025). Static analysis and topological optimization of photovoltaic panel support using recycled polymeric plastic. Advances in Science and Technology, 19(6): 167-180. https://doi.org/10.12913/22998624/203079

NOMENCLATURE

$E(T)$	temperature-dependent elastic modulus of rPA66-GF35, Pa
FoS	factor of safety
F	applied force, N
g	gravitational acceleration, m·s^{-2}
I_p	polar moment of inertia, m^4
k_b	bending stiffness, N·m
m	mass, kg
T	temperature, °C
V	volume, m^3

Greek symbols

δ	total deformation, m
σ	von Mises stress, Pa
σ_{allow}	allowable stress at temperature T, Pa
σ_{shell}	governing stress in oil-pan shell, Pa
ε	strain
ρ	material density, kg·m^{-3}

Subscripts

allow	allowable value at operating temperature
shell	quantity evaluated in the oil-pan shell
p	polar (as in polar moment of inertia)